The uniaxial strain compression of porous and fully dense beryllium

D. BEASLEY, G. I. TURNER, K. L. EDWARDS
Atomic Weapons Research Establishment, Aldermaston, Berks, UK

Compressive stress versus uniaxial compressive strain curves obtained using a simple closed die are presented for SP–100–C beryllium of initial fractional porosities varying from 0.05 to 0.26, and for fully dense ingot beryllium. The relationship between porosity and compressive yield stress is found to be linear over the entire porosity range with a discontinuity at 0.065 fractional porosity. It is suggested that the discontinuity is related to the transition from isolated to predominantly interconnected porosity.

It is deduced that the pressure required for full compaction varies with density and is estimated to range from 3.65×10^3 MN m^{-2} at 0.05 to 17.2×10^3 MN m^{-2} at 0.26 fractional porosity.

1. Introduction

Interest in beryllium is largely confined to products manufactured from powder since these combine the advantages of a near finished shape with a low texture and hence little mechanical anisotropy. Consolidation is commonly achieved by uniaxial hot-pressing but a combination of cold and hot isostatic pressing (CIP and HIP) is becoming more favoured with the increasing availability of large scale isopresses; such equipment has been recently commissioned at AWRE. The recent work, in which a simple die was used to obtain uniaxial strain compaction data for beryllium of different densities, formed part of a preliminary investigation into the mechanisms of densification during isostatic consolidation.

2. Experimental materials and methods

Specimens were cut from radiographically sound blocks of − 300 mesh SP–100–C powder hot-pressed to various densities by the established limited-ram-travel technique. After machining to the nominal size, 14.27 mm diameter × 6.35 mm high, all surfaces of each specimen were polished using ultra fine emery paper until a snug fit was achieved in the bore of the die. In all cases ovality was less than ± 0.005 mm on diameter and variations in height within ± 0.015 mm. Finally, the densities were calculated from the measurements and weights in the polished condition; see Table I.

The die set, shown in Fig. 1, and schematically in Fig. 2, comprised a tungsten carbide die 50.8 mm diameter × 22.23 mm high, shrunk into a 152.4 mm diameter tool steel bolster such that the die/bolster interface was in compression at normal stresses up to ~ 1236 MN m^{-2}; the bore of the die, (nominally 14.22 mm diameter), was highly polished to minimize wall friction effects. The anvils, also of tungsten carbide (and polished), were as short as possible consistent with the requirement for them to be used to eject the specimen. Each anvil had a tapered section circumferential groove around its heel so that during the setting-up operation it could be held lightly in position in its back plate by three radially opposed set screws, but was free to settle squarely down when the load was applied. The upper anvil back plate was located directly over the bottom fixture of the load cell. The die, which was held in a mild steel bursting ring used to axially locate the bottom anvil assembly, see Fig. 2, was supported on an annular load cell, by means of which the total downwards force due to friction was measured. This friction load cell was designed to have a higher compliance than the die-set, to be insensitive to bending moments, and to give an adequate response. The signal was fed to the y-axis of a Bryans recorder via a change-over switch which enabled either the total load or the frictional force to be displayed as required.

Owing to the complete confinement of the test piece, the measurement of its deformation was of

TABLE I Pre- and post-compaction metrology data

Specimen no.	Mean o.d. (mm)	Thickness (mm)	Weight (g)	Density (g cm^{-3})	Fractional porosity
Pre-compaction					
BC68/242/1	14.265	6.331	1.8635	1.842	0.002
B473	14.265	5.976	1.6624	1.741	0.057
B621	14.267	6.320	1.6824	1.665	0.097
B624	14.267	6.343	1.5968	1.575	0.147
HPS266	14.267	6.353	1.4846	1.460	0.208
B485	14.257	5.993	1.3039	1.363	0.261
Post-compaction					
BC68/242/1	14.293	6.313	1.8652	1.841	0.002
B473	14.310	5.694	1.6629	1.816	0.016
B621	14.316	5.823	1.6841	1.797	0.026
B624	14.319	5.560	1.5986	1.785	0.032
HPS266	14.310	5.217	1.4846	1.770	0.041
B485	14.315	4.626	1.3043	1.752	0.051

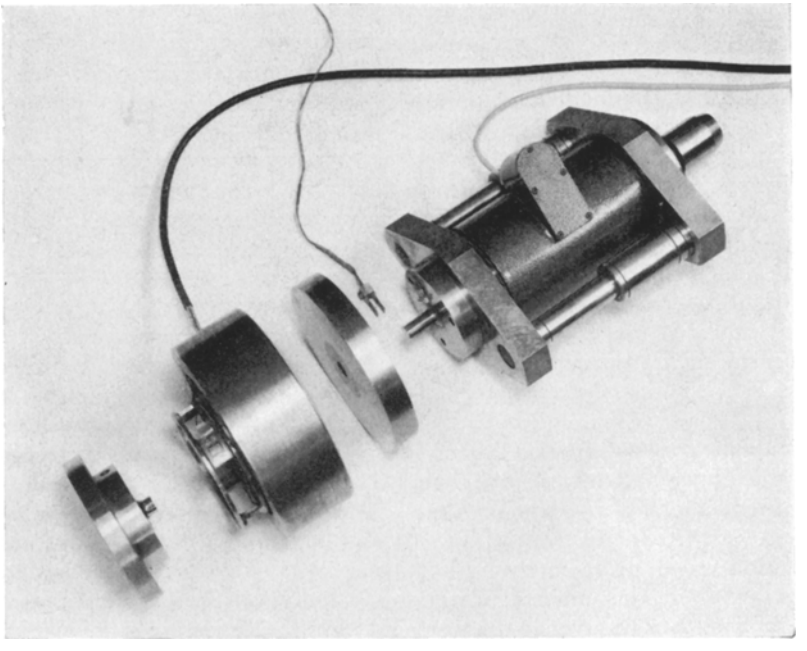

Figure 1 Exploded view of the die-set assembly.

necessity indirect. The system adopted was to measure the relative displacement of the heel of the upper anvil with respect to the die bolster, using a full bridge clip gauge located between two knife edges (Fig. 2). The output from the gauge was fed to the x-axis of the recorder. The gauge was calibrated before and after every test using a modified micrometer (0.003 mm).

After spraying the specimen and internal surfaces of the die set with PTFE to reduce frictional effects, the complete assembly was mounted on the press with the cross-head raised so that the load cell partially engaged the upper anvil. The clip gauge was then held in position between the knife edges, a small pre-load ($\sim$ 10 MN m^{-2}) applied to the specimen and the pen on the recorder zeroed for both inputs. The applied load was then increased slowly but continuously, and at regular load intervals note was made of the friction cell output; a similar

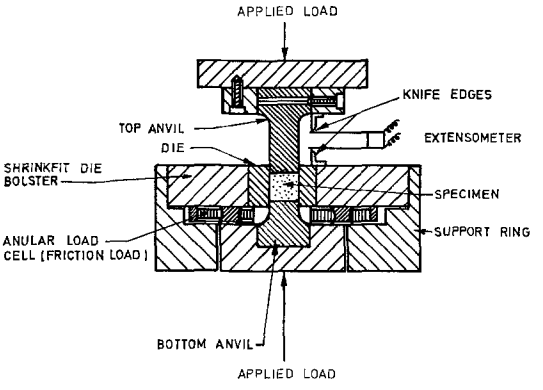

Figure 2 Sectional view of die-set.

procedure was adopted during unloading. The total time for each test was approximately 10 min.

3. Results

The results for the 90% TD specimen (Fig. 3) show the total load and frictional load versus change in height as recorded experimentally. The sources of error in this data give rise to an overestimate of both stress and strain as follows:

Stress. (a) Frictional loading between both the specimen and the anvils and the die wall. The result is that for a total applied stress σ_T and a recorded total frictional load L_F ($\equiv$ total stress loss σ_F relating L_F to specimen csa) the average stress experienced by the test piece, is given by:

$$\sigma \simeq \sigma_T - \tfrac{1}{2}\sigma_F$$

assuming approximately equal frictional stress losses at both the upper and lower anvils. In practice it was found that up to the maximum applied stress ($\sigma_T = 1.875 \times 10^3$ MN m^{-2}) the error due to friction was approximately 2%, at which level it was considered insignificant and no correction was applied. (b) The error in the load cell output is given by the calibration curve to be $\pm$ 1% at all load levels.

The care taken in specimen preparation (verified by metrology) and in the assembly of the apparatus (confirmed by reproducibility tests) was designed to minimize possible errors due to misalignment.

Strain. The errors in the recorded strain for which corrections were applied arise from the necessarily indirect means by which it was measured. This incorporates the elasticity of the die set of which the major contribution is attributable to the linear compression of the

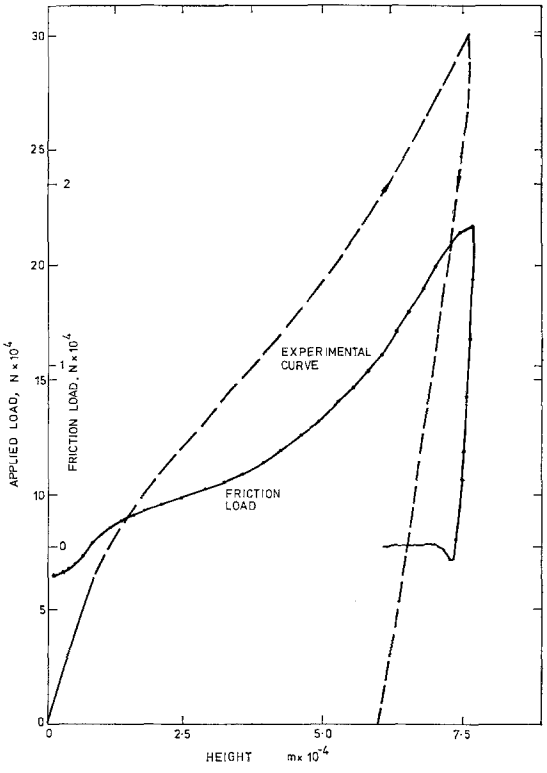

Figure 3 Experimental and friction load curves for 90% TD specimen.

anvils. The corrected stress/porosity curves for all the specimens tested are presented in Fig. 4. The pre- and post-compaction metrology data which shows the dependence of porosity upon the applied stress have been included in Table I.

4. Discussion

The shape of all the compression stress/porosity curves is similar and consistent with those associated with compaction and work hardening [1]. A notable feature is the overlap of the curves for high initial porosity with those for more dense material, indicating that although the initial compaction is easier at the high porosities it is followed by a greater resistance to compaction as consolidation proceeds. It could be anticipated from this that the pressure for full compaction should increase with initial porosity; this is confirmed by the following simple analysis.

A plot of the initial (P_i) versus the final (P_f) porosity (in the unloaded state), calculated from measurements made before and after testing is shown in Fig. 5 (the 1.875×10^3 MN m^{-2} line), together with the theoretical curve for zero

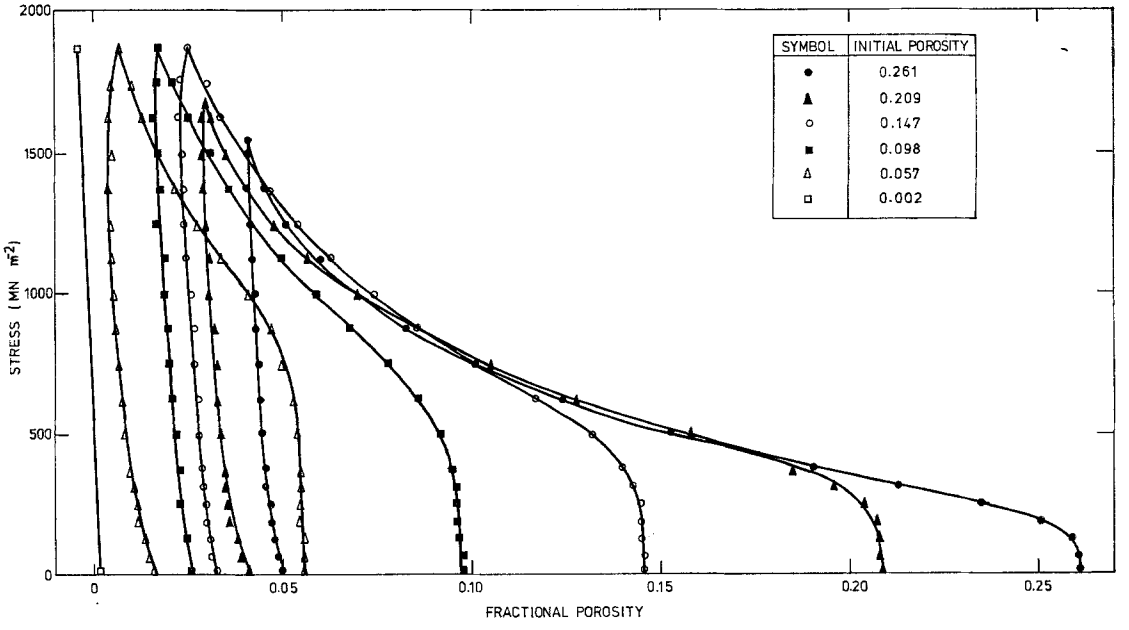

Figure 4 Compaction curves for six different porosities.

compaction and P_i/P_f data for pressures between 0.313 and 1.56 $\times$ 10^3 MN m^{-2}; the latter were derived from Fig. 4. For the maximum pressure the P_i/P_f relationship is almost linear and can be described by the simple relationship:

$$P_f = P_0 + \alpha P_i . \qquad (1)$$

However, for pressures below 1.875 $\times$ 10^3 MN m^{-2} the P_i/P_f relationship increasingly deviates from linearity indicating that as the porosity increases the compaction becomes relatively more easy, i.e. there is more compression at any given pressure. The initial slope α (Equation 1), taken as the gradient of the point of intersection of the compaction curves with the theoretical curve of zero compaction decreases from 1 for zero compaction pressure towards zero with increasing pressure.

Fig. 6 shows the relationship between the parameters P_0 and α of Equation 1 as a function of the applied pressure σ. It is apparent, despite the extended extrapolation, that the curve of P_0 versus pressure intersects the ordinate at a considerably lower pressure than does the α versus pressure curve. Referring to Fig. 5, the implication is that above a particular applied pressure (the P_0 intersect value of Fig. 6) the compaction curve intersects the P_i axis so that full compaction is attained for material with low porosity. Increasing the pressure should then result in an increase in the range of P_i values

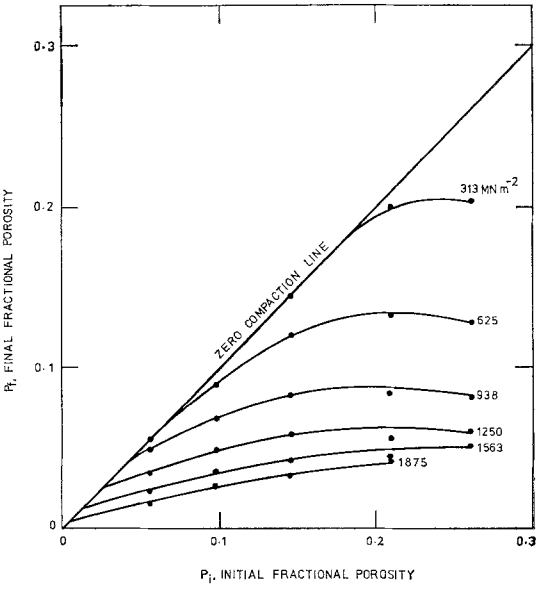

Figure 5 Relationship between initial and final porosities after loading to 1875 MN m^{-2}.

which can be fully densified, i.e. the greater the initial porosity, the greater is the pressure required for full compaction. This effect may be attributed to work hardening, evidence in support of this being provided by the post compaction hardness distributions (Fig. 7). These show that the greatest final hardness is achieved in the specimen of highest initial porosity,

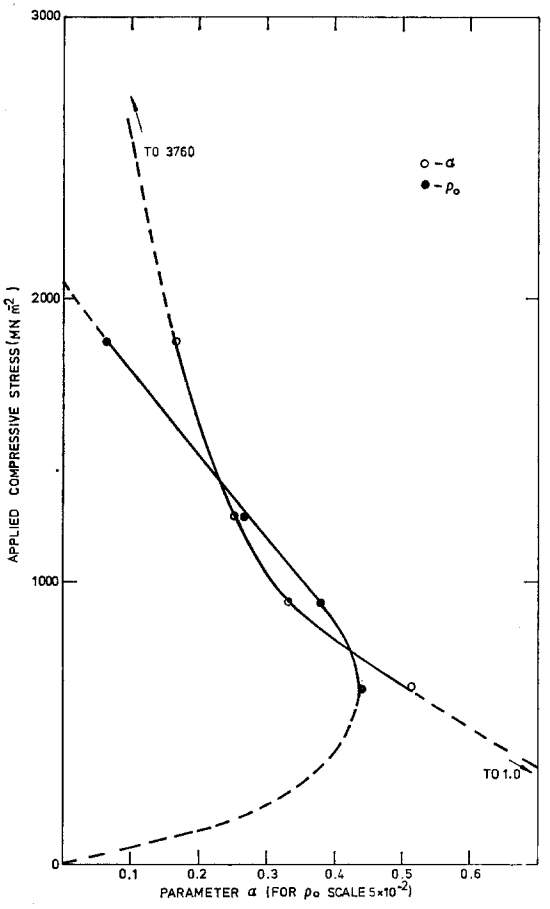

Figure 6 Dependence of the coefficients of the compaction equation upon the applied pressure.

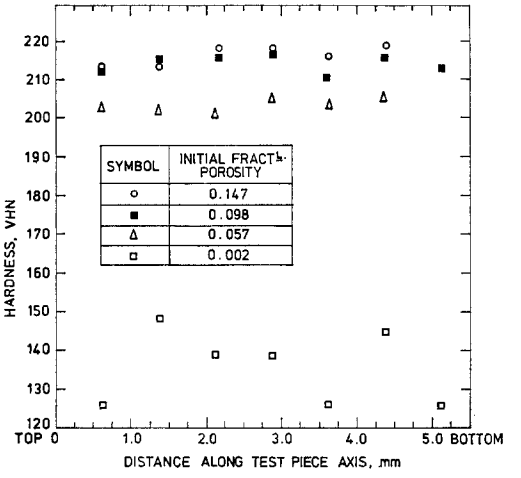

Figure 7 Post-compaction hardness distributions.

namely, post-compacted hardness of initially 85% dense specimen > that for 90% > that for 95% > that for 100%. The hardness data for the initially 74% dense specimen is omitted from Fig. 7 because the maximum stress at which it was compacted was substantially less than that applied to the other specimens. The uniformity of the hardness distributions in both radial and longitudinal directions confirmed the efficacy of the lubrication in ensuring homogeneous compaction.

The pressure required to fully densify a compact of initial porosity P_i is of considerable interest and attempts have been made to determine these pressure values both theoretically and experimentally. In the present work one derivation was attempted using the data in Fig. 5 in the following way. For any given porosity (P_i) the degree of compaction (ΔP) is given by the difference between the zero compaction curve and the compaction curve for a chosen pressure σ. The relationship between the relative compaction, i.e. $\Delta P/P_i$ and the reciprocal of the applied pressure ($1/\sigma$) at constant P_i was found to be sensibly linear for a broad range of the data as shown in Fig. 8. However, the required extrapolation of these lines to $\Delta P/P_i = 1$ did not yield a unique pressure for full compaction but instead resulted in a range of pressures corresponding to the range of P_i values such that higher pressures are required to fully compact the less dense materials. The pressures for full compaction obtained, which are approximate because of the assumed linear extrapolation, ranged from 3.65 to 17.2 $\times$ 10^3 MN m^{-2} for initial porosities of 0.05 to 0.26 respectively thus confirming the earlier observation that full compaction is more difficult to achieve the higher the initial porosity.

The yield stress versus initial porosity data derived from Fig. 4 is shown graphically in Fig. 9. The relationship is composed of two linear portions intersecting at a porosity of 0.065. At porosities greater than this value the linear relationship is similar to that previously observed for like material tested in tension, as seen by the lower, 0.5% proof stress curve in Fig. 9 [2]. However, by contrast, at porosities less than 0.065 the stress/porosity relationship in compression deviates markedly from that in tension, showing an extremely rapid increase in stress as the porosity approaches zero. It is suggested that the discontinuity in the curve occurs at that porosity which may be related to the change from mainly isolated voids to predominantly interconnected porosity [3]. The very large yield stress

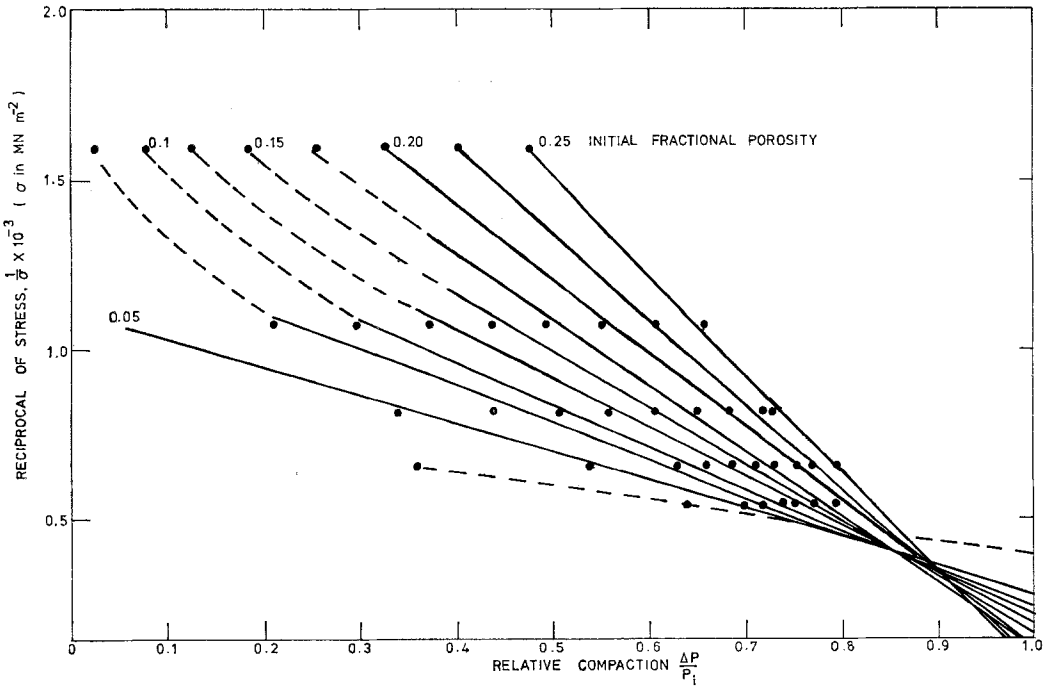

Figure 8 Relationship between relative compaction and the reciprocal of the applied stress.

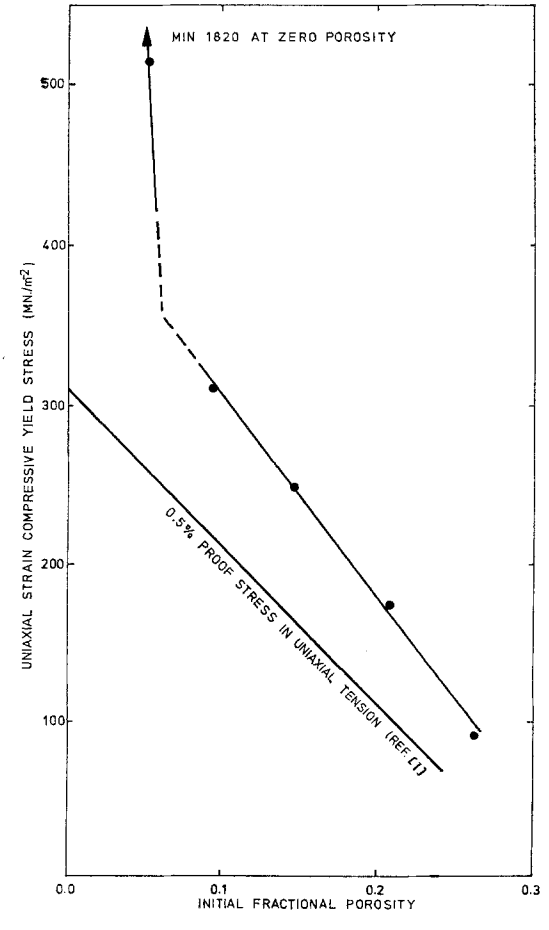

Figure 9 Flow stress as a function of porosity.

value associated with constrained fully dense material is indicative of the inability of the material to accommodate significant plastic deformation. However, it is postulated that it is necessary for only a small number of voids to be introduced to allow the material to deform plastically with a resultant sharp decrease in yield stress. The addition of further porosity will continue the decrease in yield stress in this way until a point is reached at which the porosity is largely interconnected, permitting unrestrained easy deformation similar to that reported for the tensile situation [2].

5. Conclusions

(1) For deformation in the uniaxial strain condition the relationship between porosity and compressive yield stress is linear over the range 0 to 0.26 porosity with a discontinuity at 0.065.

(2) It is proposed that the discontinuity (0.065 porosity) is related to the transition from predominantly isolated to predominantly interconnected porosity.

(3) Estimates of the pressure required for full compaction increase with increasing initial porosity ranging from 3.65×10^3 MN m^{-2} at

0.05 to 17.2 $\times$ 10^3 MN m^{-2} at 0.26 fractional porosity. This effect is attributed to work hardening.

Acknowledgement

The authors are grateful to Dr. A. J. Martin for his continued encouragement during the course of the work.

References

1. R. L. HEWITT, W. WALLACE and M. C. DE MALHERBE, *Powder Met.* **16** (31) (1973) 88.
2. R. E. COPPER, W. D. ROWLAND and D. BEASLEY, AWRE Report 025/71.
3. G. ARTHER, *J. Inst. Met.* **83** (1954) 329.

Received 29 August and accepted 18 September 1974.